



Reforecasting the November 1994 flooding of Piedmont with a convection-permitting model

Valerio Capecchi¹ 

Received: 27 March 2020 / Accepted: 6 August 2020 / Published online: 27 August 2020
© Springer Nature Switzerland AG 2020

Abstract

The Piedmont region in Italy was affected by a heavy rainfall event in November 1994. On the 4th convective cells involved the coastal mountains of the region. On the 5th and early 6th, there were abundant precipitations, related to orographic lift and low-level convergences, in the Alpine area. This study aims to evaluate whether a convection-permitting model provides more valuable information with respect to past numerical experiments. Results for the 4th of November show that the high-resolution model successfully reconstructs the structure of precipitation systems on the downstream side of the coastal mountains. As regards the precipitations of the 5th of November, no added value is found. However, we provide evidence of the anomalously intense transport of moist air from the tropical and subtropical Atlantic and postulate how such transport is responsible for reducing the stability of the flow impinging on the Alps.

Keywords Convection-permitting model · Severe weather · Past events · Reforecast

1 Introduction

Every year, weather-related disasters cause huge damage, significant economic losses and often casualties. According to the “Atlas of Mortality and Economic Losses from Weather, Climate and Water Extremes 1970–2012” edited by the World Meteorological Organization, floods and storms are the costliest events in Europe. Among such dramatic cases, the severe weather event of November 1994 in the Piedmont region (north-western Italy) is definitively one to be considered as remarkable. As a consequence of the heavy rainfall, several rivers in the southern part of the region flooded causing huge economic losses (estimated at about 14 billion US dollars) and 70 people died. Past numerical simulations were able to provide quite accurate reconstructions of the event. Nevertheless, the improvements achieved over the last 25 years in weather modelling pose the question of whether we can obtain new insights into the Piedmont flooding by using convective-scale numerical models.

✉ Valerio Capecchi
capecchi@lamma.rete.toscana.it

¹ LaMMA - Laboratorio di Meteorologia e Modellistica Ambientale per lo sviluppo sostenibile, Via Madonna del Piano 10, Sesto Fiorentino, Florence, Italy

Petrolia et al. (1996) were the first to study the November 1994 Piedmont case (hereinafter P94). They used the ECMWF global model operational at that time, both with the single deterministic forecast and with an ensemble approach. The spectral resolution of their deterministic run was T213 which roughly corresponds to about 60 km grid spacing at the Equator, while the resolution of the ensemble forecast was T63 (about 210 km). Despite the rough resolution of the model and the fact that the number of members (32 + the control member) of the ensemble was fewer than the one currently used, the authors reached some conclusions about the predictability of the event. Firstly, the day-5 to day-1 T213 forecasts were skilful, with the precipitation patterns well positioned according to observations. Secondly, the day-1 T213 forecast provided a rainfall maximum of 135 mm, which, although strongly underestimated with respect to observed data, gave a clear warning of potential severe weather. Finally, the evolution of rainfall predictions in the day-8 to day-3 T63 simulations exhibited consistency, suggesting a significant possibility of an extreme event in the grid point closest to the area of interest. The authors concluded that the probabilistic T63 predictions supported the results of the deterministic T213 forecast and reinforced the degree of confidence that could be associated with it.

Analysing the data registered by automatic weather stations, on the 4th of November, intense rainfall rates affected southern Piedmont, in an area between the Maritime Alps and Ligurian Apennines (Lionetti (1996); Jansa et al. (2000); Cassardo et al. (2002)). Buzzi et al. (1998) noted how large errors in their numerical experiments were associated to precipitation forecasts in southern Piedmont, where convection was the main contributor to rainfall. They concluded that these errors were likely due to the lack of an explicit computation of the trajectories of convective cells. A misplacement of precipitation maxima in this area was also found in the work by Ferretti et al. (2000). In another paper, Buzzi and Foschini (2000) implemented a high-resolution model simulation of the P94 case adopting the parametrisation approach to convection even at mesh size close to the hydrostatic limit (4 km). Also in this case, the authors demonstrated how the precipitation maxima over southern Piedmont were underestimated and misplaced by about 25–30 km to the south of the actual position. As a consequence, the drainage basins of the Tanaro, Bormida and Belbo Rivers in southern Piedmont would not be affected by rainfall runoff with likely errors in hydrological predictions.

Romero et al. (1998) used the hydrostatic mesoscale model described in Nickerson et al. (1986) to analyse the P94 case. Numerical simulations agreed well with observed precipitation patterns; however, maximum rainfall predictions were strongly underestimated. By looking at the convective part of the simulated precipitation, the authors argued that the rainfall over Piedmont on the 5th of November had a non-convective nature.

This assessment was confirmed by Doswell III et al. (1998) who analysed satellite images. They concluded that much of the rainfall over the foothills of the Alps in the Piedmont area was associated with upslope flow of weakly stable, moist air. Furthermore, using the ECMWF analysis data, they calculated the Froude number, defined by the relationship

$$Fr = \frac{U}{Nh}, \quad (1)$$

where U is the horizontal wind speed averaged over the 1000-, 925-, and 850-hPa isobaric levels; N is the stability Brunt-Väisälä frequency calculated from the potential temperature difference between 1000- and 850-hPa levels and h is the height of the orography (which is about 3000 m in the case of the western Alps). When the Froude number is greater than 1, flow over the orographic obstacle is favoured, thanks to strong low-level winds U or to reduced values of the static stability N (or a combination of the two). On the contrary, the

ascent is reduced when $Fr \ll 1$, favouring flow around the obstacle (depending on the geometry of the mountains). Doswell III et al. (1998) found that the Froude number was about 0.90 on the 5th of November. They concluded that in this regime, the uplift flow could be attained only in saturated conditions.

In their idealised numerical study with an L-shape orography (rotated 90° clock-wise), Rotunno and Ferretti (2001) demonstrated how westward deflection of the southerly sub-saturated flow blocked by the eastern Alps enhanced low-level convergence with the saturated flow directed towards the western Alps. As a consequence, this latter flow was forced to ascend further upstream the mountainous barrier, due to the difference of equivalent potential temperature between the two airflows (see Figure 16 in their paper).

Similar considerations are found in Buzzi et al. (1998). To demonstrate how a relatively stable and moist flux can change the Froude number, they conducted some experiments to assess the role of latent heat exchanges due to condensation and evaporation. A numerical investigation was conducted by suppressing latent heat release due to condensation. Results showed that the low-level flow over the Mediterranean Sea was diverted to the western side of the Alps with respect to the control simulation. As a consequence, the precipitation maxima were found in southern France (see Figures 12 and 13 in their paper). To explain such behaviour, the authors underlined that suppressing the release of latent heat due to condensation resulted in higher mean sea level pressure values in the Alpine region and thus a reduced uplift flow over the mountains. Similar findings and discussions are reported in Ferretti et al. (2000).

Moreover, Buzzi et al. (1998) and other authors (Romero et al. (1998); Ferretti et al. (2000); Jansa et al. (2000); Cassardo et al. (2002)) performed numerical experiments by suppressing (or reducing) the orography of the model grid. All of them found that the precipitation maxima were strongly reduced. Findings in the literature showed that on the 5th of November, the precipitation in the Alps (northern Piedmont) was the result of the combined action of orographic uplift and latent heat exchanges and that convection played a marginal role.

Table 1 lists past numerical experiments dealing with the P94 case. All the models deployed some kind of parametrisation scheme for convection processes. Mesh sizes ranged between 60 km for the global model used in Petroliaigis et al. (1996) and 4 km, which is the resolution of the experiments by Buzzi and Foschini (2000).

An analysis of the P94 case can be conducted in light of an atmospheric river (AR) land-fall. Since the seminal work by Zhu and Newell (1998), AR theory and field experiments

Table 1 Past numerical investigations on the November 1994 Piedmont case

Reference	Model	Resolution (grid spacing)	Vertical levels	Forecast length
Petroliaigis et al. (1996)	IFS Deterministic	T213 (\simeq 60 km)	31	120 h
"	IFS Ensemble	T63 (\simeq 210 km)	19	120 h
Romero et al. (1998)	SALSA	20 km	30	30 h
Buzzi et al. (1998)	BOLAM	30 and 10 km	36	36 h
Buzzi and Foschini (2000)	BOLAM	40, 10 and 4 km	28, 38 and 40	48, 42 and 30 h
Jansa et al. (2000)	HIRLAM	40 km	31	48 h
Ferretti et al. (2000)	MM5	30 and 10 km	23	48 h
Cassardo et al. (2002)	RAMS	15 km	35	84 h

have received much attention in relatively recent years (see for instance Ralph et al. (2004), Lavers and Villarini (2013) and Krichak et al. (2016)). Roughly speaking, ARs are defined as narrow tongues of moist air in the lower troposphere responsible for the transport of tropical water vapour into the extratropics. Although ARs are mainly studied for their impacts on the western coasts of the USA, some papers demonstrated that heavy precipitation and flood events in Europe are often linked to AR landfall (Stohl et al. (2008), Lavers and Villarini (2013), Krichak et al. (2016)). Furthermore, as stated in Krichak et al. (2016), the regions mostly prone to the impacts of AR landfall are mountainous, providing the necessary uplift for significant rainfall.

Over the last few decades, convective-scale numerical weather prediction modelling improved tremendously (Sun et al. 2014) and is now facing new challenges. In fact, it is not automatic that higher-resolution models will provide more accurate predictions, because of the lack of basic understanding of some theoretical and practical issues regarding the convective-scale regime. To mention a few, we recall cloud microphysics, turbulence and numerics (see Yano et al. (2018) for a complete list). Nowadays, the predictability of small-scale, high-impact weather remains limited due to (i) approximations in the reconstruction of fine-scale processes (Leutbecher et al. 2017) and (ii) the chaotic nature of the weather system causing small errors in the initial conditions to grow rapidly (Palmer 2001). Nowadays, technological capability allows operational convection-permitting models to be run with horizontal mesh sizes less than 2 km as well as ensemble systems with horizontal mesh size about 3 km. To mention a few examples in national weather services in Europe, the mesh size of the operational model of Météo-France (AROME) is about 1.3 km; the UK Met Office runs a 1.5-km grid length model four times per day and has plans to deploy a sub-kilometre scale version in the near future. The newest version of the ICON model at the German DWD weather service is a seamless model that can be run with a mesh size of less than 1 km. As regards probabilistic prediction systems, examples include COSMO-DE at 2.8 km horizontal resolution (Peralta et al. 2012), MOGREPS-UK at 2.2 km horizontal resolution (Hagelin et al. 2017) and AROME-EPS at 2.5 km horizontal resolution (Raynaud and Bouttier 2016).

The goal of this paper is to perform a reforecast of the P94 case. We present a numerical reconstruction by applying cutting-edge regional convection-permitting NWP modelling, fed by recently updated global analyses. The purpose is twofold: as regards the rainfall observed on the 4th of November, the challenge is to improve the prediction of the convective precipitations in southern Piedmont, where the majority of damage and casualties occurred. As regards the rainfall observed on the 5th of November, we provide evidence of an AR landfall during the days of the P94 case. In addition, we investigate if a better quantitative precipitation forecast can be accomplished by deploying a high-resolution model, which uses an accurate description of topography.

We conclude this introduction by stressing the fact that reforecasting past high-impact events is a valuable tool to assess if operational numerical weather models are improving over time, by comparing the results we achieve nowadays with those obtained in the past.

The paper is organised as follows: Section 2 provides a description of the synoptic situation of the event, Section 3 describes the limited-area model and the initial and boundary data used for the simulation. Moreover, it is presented an algorithm for the detection of AR conditions. In Section 4, we show quantitative precipitation forecast and its verification using rain-gauge data as ground truth. In Section 5, we discuss the results and provide some new insights of the P94 dynamics, in light of an AR landfall.

2 Synoptic overview

Although detailed synoptic descriptions of the P94 case can be found in the papers listed in Table 1, we include here a short summary to make this paper self-contained. October 1994 was characterised by a remarkable weather variability over north-western Italy. Accumulated rainfall recorded by automatic weather stations was above average in several districts of Piedmont. Between the 2nd and 4th of November, there was an upper-level cyclonic circulation over the northern Atlantic area (Petroliagis et al. 1996). ERA5 data valid at 12 UTC of the 4th of November show a trough with an axis extending from the British Isles to the Iberian peninsula (see Fig. 1a).

This configuration activated the advection of warm and moist air over the western/central Mediterranean Sea towards southern France and northern Italy. As recorded by rain-gauges data (Lionetti 1996), this time practically coincided with the beginning of the heavy precipitations in southern Piedmont. For instance, see in Fig. 2a the accumulated precipitation recorded at the Ponzone rain-gauge (whose location is indicated in Fig. 3).

One day later, the movement of the trough eastwards was slow, due to the ridge present over the central/eastern Mediterranean Sea and Europe (see Fig. 1b). As a consequence, a double front-like structure formed west of Italy as confirmed by numerical simulations and Meteosat satellite images (Buzzi et al. (1998); Doswell III et al. (1998)). This configuration is not uncommon in the western Mediterranean; see for instance the discussions in Buzzi et al. (1998) and Porcú et al. (2003). It is often associated, as in the P94 case, with intense

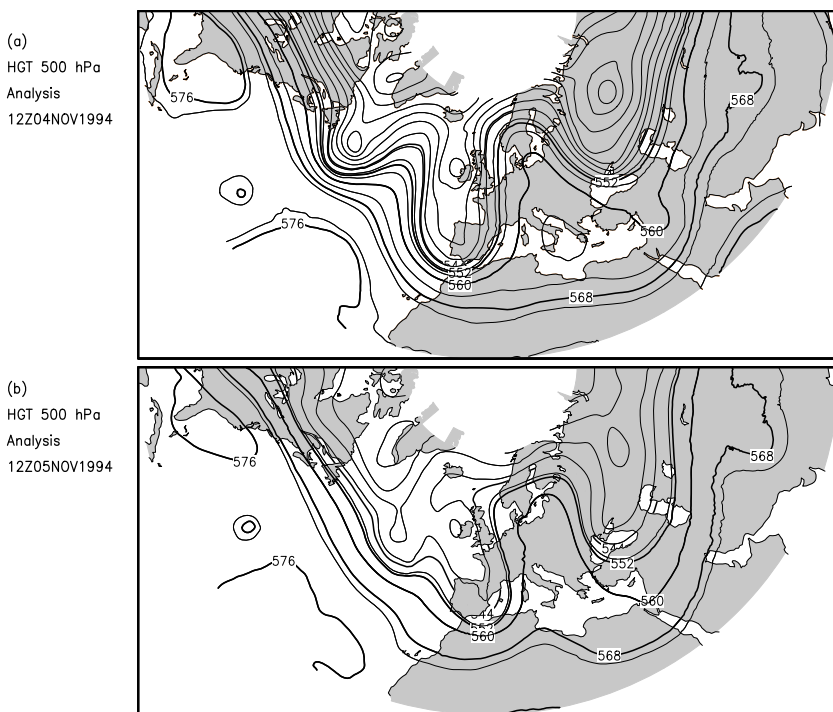


Fig. 1 Analysis maps of geopotential height at 500-hPa level valid at **a** 12 UTC on 4 November 1994 and **b** 12 UTC on 5 November 1994. ERA5 data were used to produce the plots

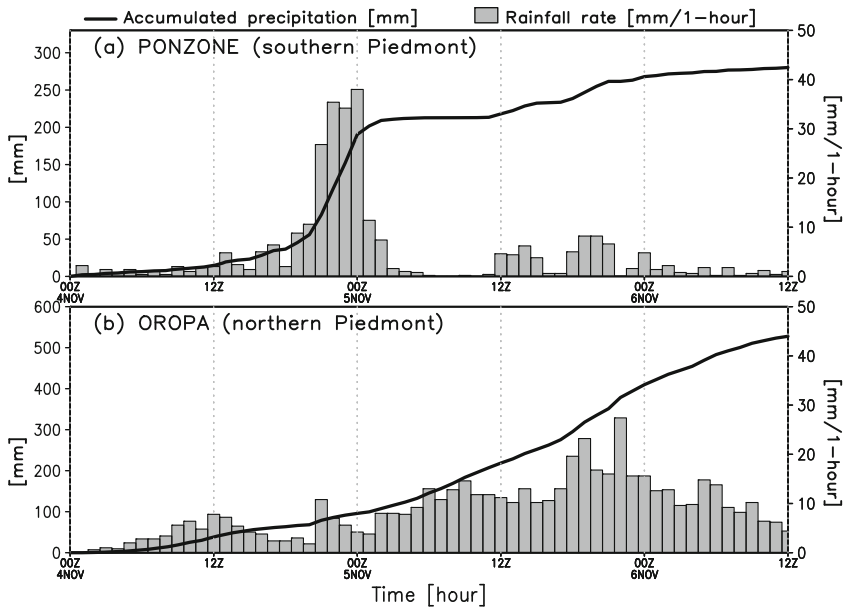


Fig. 2 Accumulated precipitations recorded in the period from 00 UTC 4th November 1994 to 12 UTC 6th November 1994 by the raingauges at Ponzone **(a)** and Oropa **(b)**, whose geographical positions are shown in Fig. 3

precipitations in the Alpine region; see the plots in Fig. 4 of Lionetti (1996) and the accumulated precipitation recorded at Oropa rain-gauge in Fig. 2b. We note how rainfall rates at Oropa reached 27 mm h^{-1} with an average value on the 5th of November about 10 mm h^{-1} . Instead, data recorded at Ponzone (Fig. 2a) reported a maximum value of 38 mm h^{-1} with about 135 mm in the last 4 h of the 4th of November. Thus, the profiles of precipitation rates of Ponzone rain-gauge (southern Piedmont) exhibited much higher time variability, indicating the presence of convection. This assessment is also found in Buzzi et al. (1998).

We conclude this brief overview of the P94 case by stressing the fact that, as demonstrated by the numerical experiments conducted by Romero et al. (1998) and Cassardo et al. (2002), the contribution to the precipitations of the Mediterranean sea surface evaporation was likely not important.

3 Model and methods

3.1 Model description

In this paper, we present high-resolution simulations of the P94 case performed using the Meso-NH model. This is a French research community model, jointly developed by the Centre National des Recherches Météorologiques (CNRM) and Laboratoire d'Aérodynamique (LA) at the Université Paul Sabatier (Toulouse). It is designed to simulate the time evolution of several atmospheric variables ranging from the large meso- α scale ($\simeq 2000 \text{ km}$) down to the micro- γ scale ($\simeq 20 \text{ m}$), typical of the Large Eddy Simulation (LES) models. For a general overview of the Meso-NH model and its applications, see Lac et al. (2018), while the

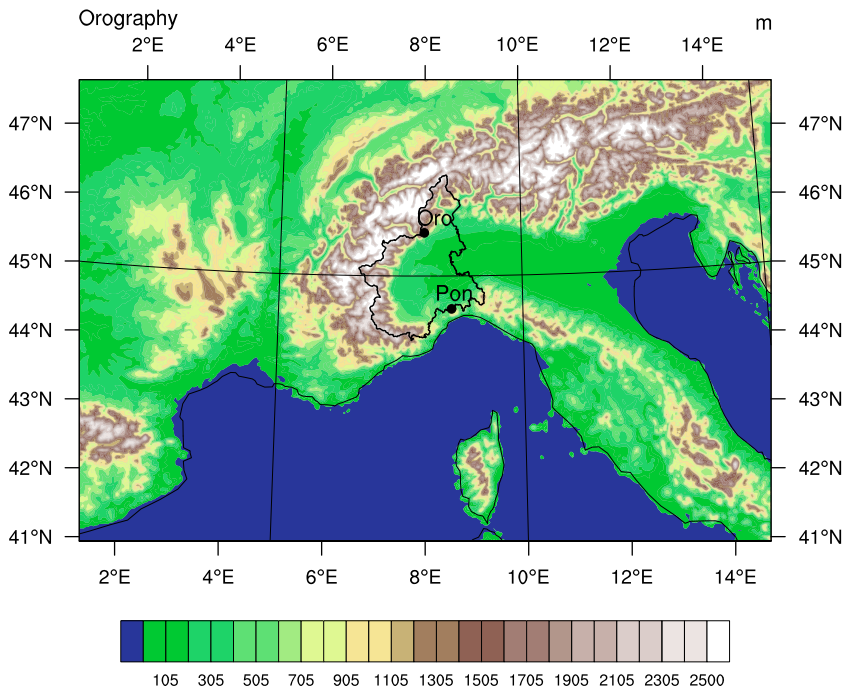


Fig. 3 Orography of the domain of the Meso-NH simulation. Horizontal grid spacing Δx is 2.5 km. The locations of the Oropa (“Oro”) and Ponzone (“Pon”) rain-gauges are indicated by black dots. The political borders of the Piedmont region are indicated by the black line

scientific documentation is available on the model’s website (<http://mesonh.aero.obs-mip.fr>). For this study, we used the version 5.4.1 (released in July 2018). The geographical extent of the simulations is shown in Fig. 3; no grid-nesting was implemented. As regards microphysics, we set the one-momentum ICE3 scheme (Caniaux et al. 1994) that takes into account five water species (cloud droplets, raindrops, pristine ice crystals, snow or aggregates, and graupel). The grid spacing (Δx) was set to 2.5 km and the parametrisation of convection processes was turned off, because such resolution allowed part of the convection processes to be treated explicitly (Hohenegger et al. 2008). The Runge-Kutta-centred 4th-order scheme was chosen for momentum advection. This scheme is recommended when using, as in the present paper, the CENT4TH (4th order CENTred on space and time) advection scheme. The CENT4TH was chosen because of its numerical stability, although it is more time-consuming than other options (Lunet et al. 2017). Some specific parameters of the model for this study are summarised in Table 2.

To drive the Meso-NH simulations, global data were produced using the ECMWF-IFS global model. Two datasets were disseminated with different settings: the first one (labelled “h6bg”) made use of the model cycle 45r1, which was operational in June 2018. Its spectral resolution is TCO1280 which roughly corresponds to 9 km grid spacing. It consists of both analyses, generated every day at 00 UTC from the 1st to the 7th of November, and forecast data; forecast length is 72 h. The second dataset (labelled “3738”) was created using the model cycle 41r2 and used the ERA5 setup. It consists of analyses produced every hour from the 1st of October to the 14th of November. It has a grid spacing (about 18 km) higher than ERA5 data. In our numerical experiments, the Meso-NH forecasts were started by using

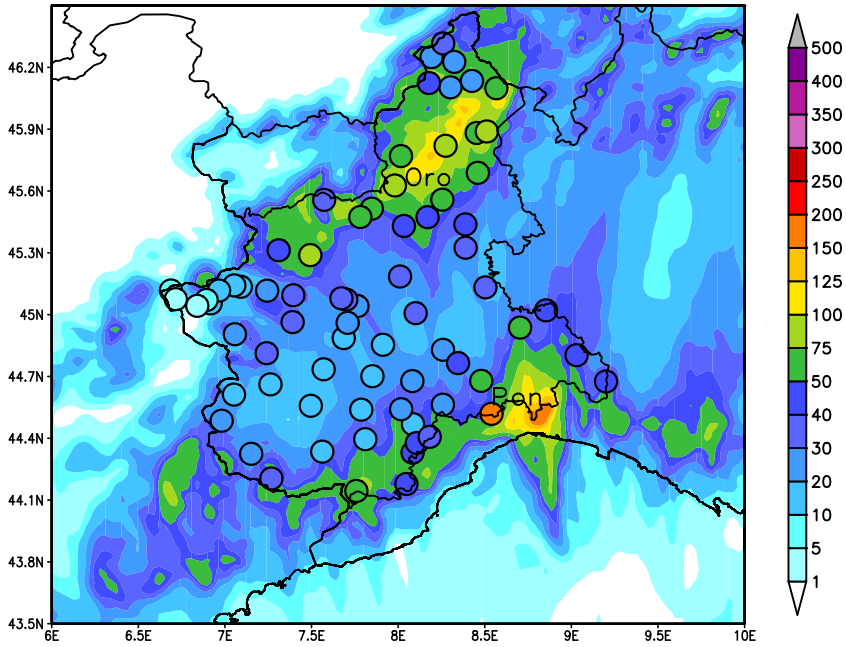


Fig. 4 QPF data for the precipitation accumulated in the 24-h period ending at 00 UTC on the 5th of November. The forecast is initialised at 00 UTC on the 4th of November. Observed values overlap forecast data and are indicated with the coloured circles

both the “h6bg” and “3738” datasets, with boundary conditions passed every 3 h. However, we present only the results driven by the “h6bg” dataset, because the results do not differ substantially and because we want to mimic an operational-like forecasting system.

3.2 Methods

As proposed in the seminal work by Zhu and Newell (1998), ARs can be detected by looking at the vertically integrated horizontal water vapour transport (hereafter, integrated vapour transport, IVT) defined as

$$IVT = \sqrt{\left(\frac{1}{g} \int_{p_0}^{p_{top}} qu dp\right)^2 + \left(\frac{1}{g} \int_{p_0}^{p_{top}} qv dp\right)^2}$$

Table 2 Key parameters of the Meso-NH model settings

Variable	Value
Rows×columns	300×450
Horizontal grid spacing	2.5 km
Vertical resolution	52 levels (up to 20 km)
Time step	10 s
Cumulus convection	Explicit (no parametrisation)
Microphysics option	ICE3 scheme (Caniaux et al. 1994)

where $q(p)$ is the specific humidity in $kgkg^{-1}$, $u(p)$ and $v(p)$ are the zonal and meridional components respectively of the horizontal wind vector in ms^{-1} , g is the acceleration due to gravity, and p_0 and p_{top} are the 1000- and 300-hPa isobaric levels respectively. The algorithms based on this approach (Rutz et al. 2014) declare grid points as interested by an AR if they satisfy the condition that IVT exceeds a predefined threshold, which is normally equal to $250 kg m^{-1}s^{-1}$. Ralph et al. (2019) proposed a scale to characterise the strength and impacts of ARs. It is based on the analysis of both the maximum value of IVT at a given location during the AR event (i.e. $IVT \geq 250 kg m^{-1}s^{-1}$) and the AR duration. We underline that the definitions of AR condition and duration are in the Eulerian sense, namely they apply to fixed points.

The IVT maps presented in Figs. 9 and 10 were calculated using the ERA5 data (Hersbach et al. 2019).

Quantitative precipitation forecasts (QPF) provided by the Meso-NH simulation are compared with daily rainfall amounts observed at automatic weather stations in the Piedmont region. The total number of rain-gauges is 80 for the 4th and 78 for the 5th of November. To avoid misleading information, we exclude from the analysis those stations whose altitude is greater than 2000 m, because snowfall was reported in mountainous areas at approximately 2400 m above sea level (Lionetti 1996).

To mitigate the effects of the double-penalty error (Ebert 2009), when extracting the QPF values at rain-gauge locations, we picked the four nearest-neighbor grid values and averaged them to provide the forecast value at that location. Standard verification statistics are considered: root mean square error (RMSE), mean absolute error (MAE), multiplicative bias (bias) and the square of Pearson’s correlation coefficient (see Wilks (2011) for the definitions). Furthermore, to summarise multiple aspects of the model performance in a single diagram, we make use of the performance diagrams (Roebber 2009). Such diagrams plot four measures of dichotomous forecast: probability of detection (POD), success ratio (SR), frequency bias and critical success index (CSI). Using the 2×2 contingency table for dichotomous (yes/no) forecast shown in Table 3,

the four skill measures are defined as follows:

$$\begin{aligned}
 POD &= \frac{A}{A + C}, \\
 SR &= 1 - \frac{B}{A + B}, \\
 bias &= \frac{A + B}{A + C}, \\
 CSI &= \frac{A}{A + B + C}.
 \end{aligned}$$

Table 3 The 2×2 contingency table

		Event observed	
		Yes	No
Event forecast	Yes	A	B
	No	C	D

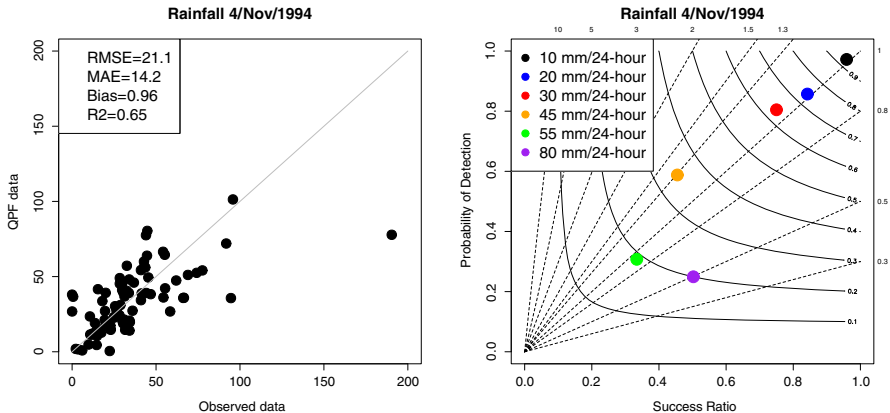
4 Results

In Fig. 4, we show the 24-h accumulated precipitations predicted by the Meso-NH model for the 4th of November. Observed amounts (coloured circles) overlap the forecasts data. Starting time of the simulation is 00 UTC 4 November 1994. Forecasts initialised one and two days in advance do not provide substantial differences to the one shown here.

From the visual inspection of Fig. 4, the pattern of precipitation forecast is in good agreement with observed values. However, the simulation tends to slightly overestimate rainfall along the coastal mountains (that is in southern Piedmont). As regards the comparison with the rainfall registered at Ponzone rain-gauge, the four grid points closest to that station provide QPF values that are lower than the observed value. However, a local QPF maximum is found approximately 20 km to the east of the Ponzone location.

To estimate how accurate is the model simulation, in Fig. 5a, we show the scatter plot of the QPF values against observations, with standard verification statistics reported in the upper-left corner. In Fig. 5b, we show the performance diagram for selected rainfall thresholds corresponding to approximately the 10th, 25th, 50th, 75th, 85th and 95th percentiles of the observational dataset.

From Fig. 5a, we can appreciate a good agreement (that is $R^2 > 0.65$) between predicted and observed rainfall data. However, forecasts slightly underestimate observations because the multiplicative bias is less than 1. Both RMSE and MAE are moderate, and are further reduced to approximately 15 and 13 mm if we discard the Ponzone value, which represents the outlier of the observational dataset. The performance diagram in Fig. 5b suggests that the predictions are accurate up to the 30-mm threshold (the points are close to the upper-right corner), which represents the 50th percentile of the observational dataset. Then, the performance of the model decreases and the forecasts provides poor results in particular



(a) Scatter plot between observed precipitations and Meso-NH QPF data

(b) Performance diagram for the rainfall thresholds 10 (black), 20 (blue), 30 (red), 45 (orange), 55 (green) and 75 (purple)

Fig. 5 a: scatter plot of observed vs predicted rainfall data for the 4th of November 1994. In the top-left inset rectangle, we report the root mean square error (RMSE), the mean absolute error (MAE), the multiplicative bias (Bias) and the square of Pearson's correlation coefficient (R^2). b: performance diagrams for the 4th of November. The X-axis shows the success ratio (SR), the Y-axis shows the probability of detection (POD), the curved lines represent critical success index (CSI) values, and the dashed diagonal lines represent bias

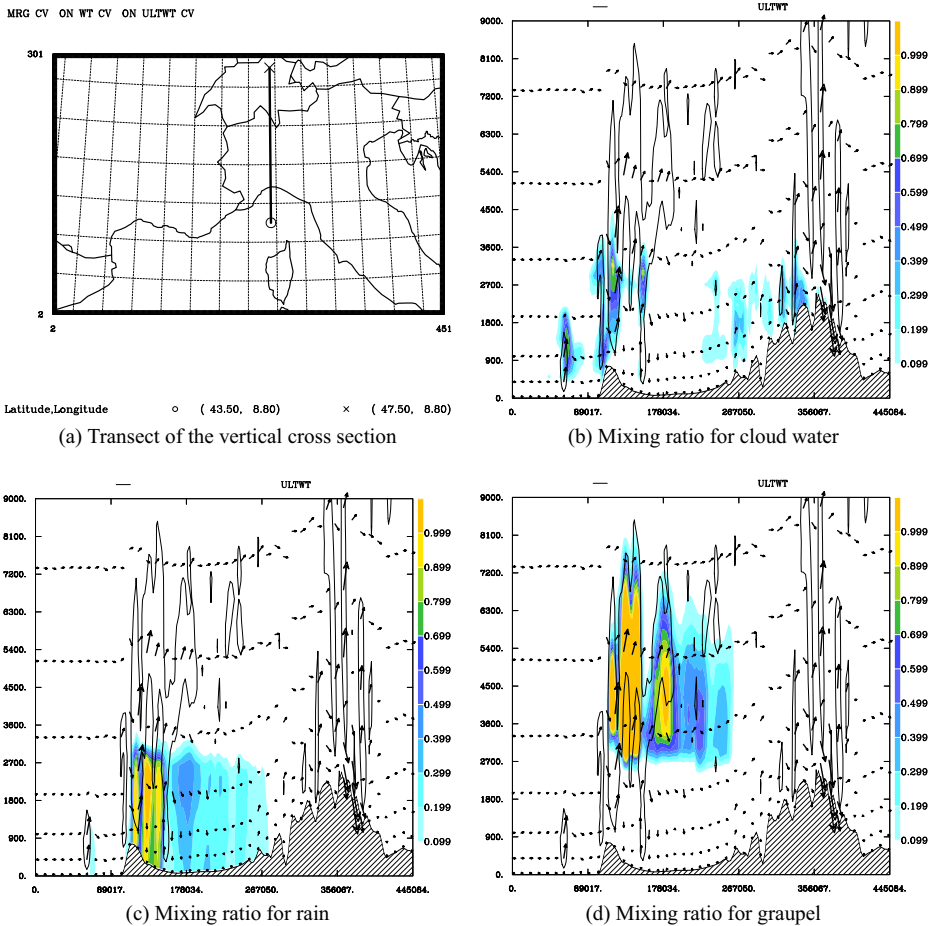


Fig. 6 Vertical cross section of the Meso-NH forecast valid at 13 UTC of the 4th of November. In panels **b–d**, wind vectors overlap the mixing ratios (unit is $kgkg^{-1}$) of three classes of hydrometeors: **b** cloud water, **c** rain and **d** graupel. Contour intervals indicate vertical velocities greater than 1 ms^{-1} . The transect is in panel **a**. On the X-axis of panels **b–d** is indicated the distance (in m) from the starting point (○ symbol in panel **a**) of the transect whereas on the Y-axis the altitude in m is indicated. The model orography is dashed

for the 55-mm and 80-mm thresholds, which represent the 85th and 95th percentiles of the observed data.

In Fig. 6, we show the vertical cross section at 13 UTC of the 4th of November of a transect (indicated in panel Fig. 6a) close to the Ponzzone rain-gauge. The panels in Fig. 6b, c and d show the mixing ratio of cloud droplets, rain and graupel respectively and the wind vectors at selected model levels.

Convection is visible on the lee side of the coastal mountains associated to moderate to strong vertical velocities. The model reconstructs a vertical structure of liquid and ice hydrometeors up to mid-troposphere and above. The freezing level is at about 3000 m, and the value agrees well with the data observed at the sounding station of Milano Linate airport (located about 50 km to the east of the transect), which reported a freezing level at about 3100 m.

In Fig. 7, we show the 24-h accumulated precipitations predicted by the Meso-NH model for the 5th of November. Observed rainfall data overlap predictions and are indicated with the coloured circles. Starting time of the simulation is 00 UTC 5 November 1994. Forecasts initialised one and two days in advance do not provide any substantial difference to the rainfall map presented here. From the visual inspection of Fig. 7, we note that Alps seem to be unrealistic with values up to 500 mm or more in correspondence with mountain peaks.

To evaluate quantitatively the accuracy of the simulation, we compared the 24-h rainfall amounts recorded by the rain-gauges located in the Piedmont region (shown in Fig. 7 with the coloured circles) with the predictions. The scatter plot and standard skill scores are reported in Fig. 8a. The agreement is good ($R^2 > 0.72$) and similar to what is found for the 4th of November, whereas the model tends to slightly overestimate the precipitations (the bias is greater than 1). The RMSE and MAE errors are greater than those found for the previous day (compare the values reported in the inset rectangles of Figs. 5a and 8a); however, we have to take into account that the mean of the observed data is approximately 100 mm. As regards the performance diagram shown in Fig. 8b, all the points lie close to the diagonal and are closet to the upper-right corner up to the 50-mm rainfall threshold. As expected, the higher the threshold, the poorer the score, although the scores corresponding to the 85th and 95th percentiles (that is 200 mm and 250 mm) are better than those found for the 4th of November (compare Figs. 5b and 8b).

In Figs. 9 and 10, we show the IVT maps for the four 6-h steps of the 5th and 6th of November respectively. On the 5th of November (Fig. 9), an elongated band of moisture transport connects the coasts of northern Africa to the British Isles, involving part of the Italian peninsula and France. This band is about 2100 km long and 500 km wide. Elevated

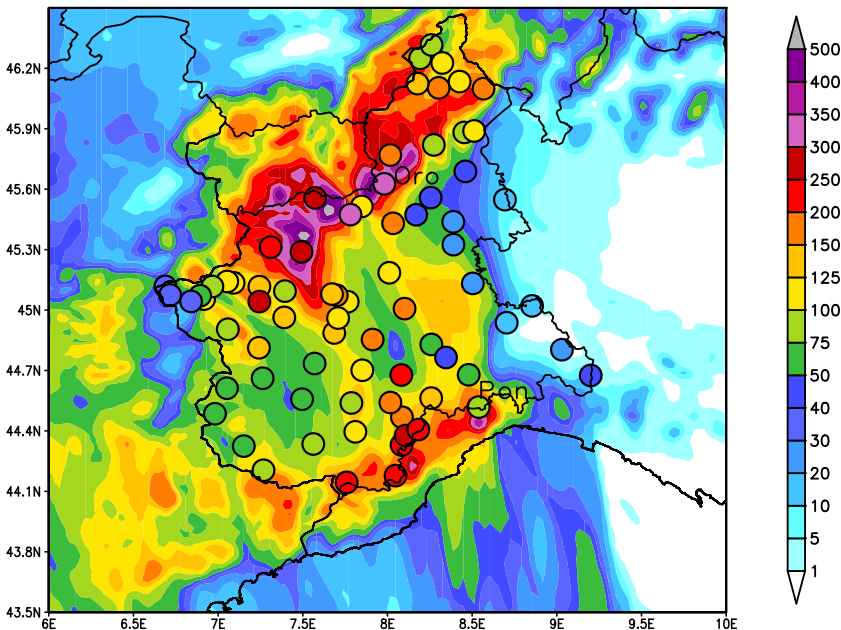
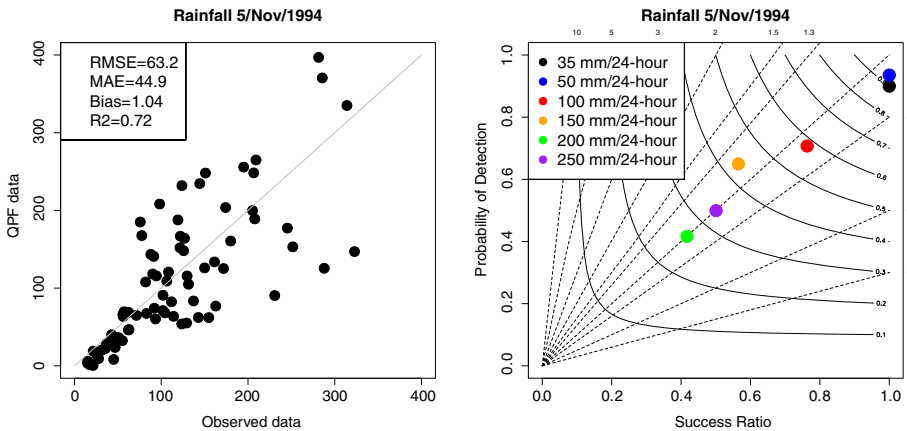


Fig. 7 QPF data for the precipitation accumulated in the 24-h period ending at 00 UTC on the 6th of November. The forecast is initialised at 00 UTC on the 5th of November. Observed values overlap forecast data and are indicated with the coloured circles



(a) As in Figure 5a but for the 5th of November

(b) As in Figure 5b but for the 5th of November and for the rainfall thresholds 35 (black), 50 (blue), 100 (red), 150 (orange), 200 (green) and 250 (purple)

Fig. 8 **a:** scatter plot of observed vs predicted rainfall data for the 5th of November 1994. In the top-left inset rectangle, we report the root mean square error (RMSE), the mean absolute error (MAE), the multiplicative bias (Bias) and the square of Pearson's correlation coefficient (R2). **b:** performance diagrams for the 5th of November. The X-axis shows the success ratio (SR), the Y-axis shows the probability of detection (POD), the curved lines represent critical success index (CSI) values, and the dashed diagonal lines represent bias

IVT values, greater than the critical threshold of $250 \text{ kg m}^{-1} \text{ s}^{-1}$, are found in the area of interest, which is indicated in the plots with a red rectangle. On the 6th of November, this moist corridor is split in two parts: one to the north of the Alps and one to the south. However, we can still observe high values of IVT ($\geq 250 \text{ kg m}^{-1} \text{ s}^{-1}$) in the north-eastern part of the Piedmont area, at least in the early part of the day (i.e. until 06 UTC). Following the intensity scale proposed by Ralph et al. (2019), we note that for selected pixels in the southern and eastern part of the Piedmont area this yields the following: (i) AR conditions (i.e. $IVT \geq 250 \text{ kg m}^{-1} \text{ s}^{-1}$) lasted for at least 24 h (see the maps in Figs. 9b–d and 10a) and (ii) maximum instantaneous IVT values exceeded $600 \text{ kg m}^{-1} \text{ s}^{-1}$ on the 5th of November (plot not shown). We can thus classify the AR that involved the P94 case as category 2 out of 5 categories following Ralph et al. (2019).

5 Discussions and conclusions

To commemorate the twenty-fifth anniversary of the Piedmont flooding, we revisited the P94 case by applying cutting-edge regional NWP modelling. High-resolution simulations were forced by initial and boundary conditions produced ad hoc with a recent version of the ECMWF-IFS global model. The goal of the work was twofold: firstly, we wanted to investigate whether a convection-permitting model is able to reconstruct the pre-frontal convection activity observed on the 4th of November in southern Piedmont. Secondly, as regards the orographic precipitation on the 5th of November in the Alpine area, we wanted to assess any new insights of a high-resolution simulation. In fact, previous studies used numerical weather models, with the parametrisation of convection processes and mesh sizes in the order of few tens of kilometres or near the hydrostatic limit (Buzzi and Foschini 2000).

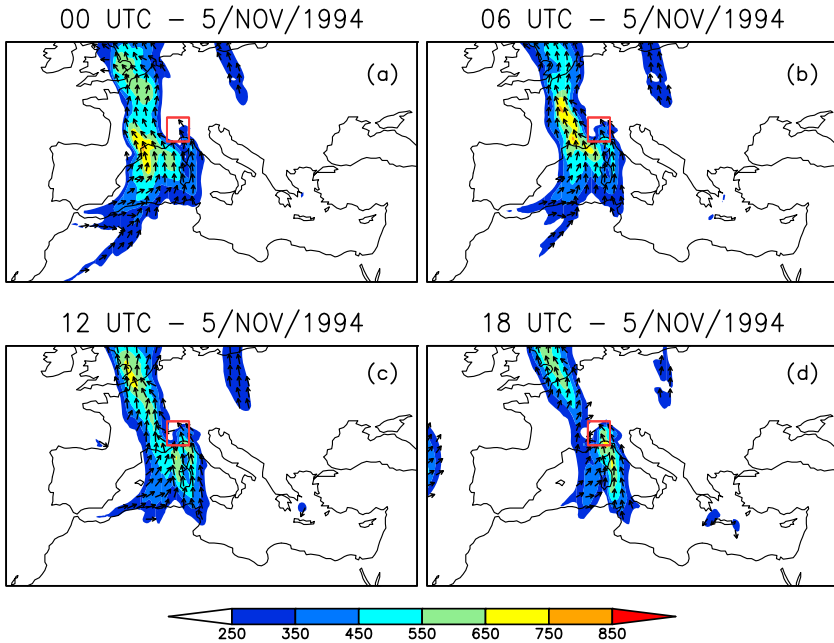


Fig. 9 Vertically integrated horizontal water vapour transport (IVT) values expressed in $kg\ m^{-1}\ s^{-1}$ for the four 6-h time steps on the 5th of November 1994: **a** 00 UTC, **b** 06 UTC, **c** 12 UTC and **d** 18 UTC. Wind vectors at 850-hPa isobaric level are plotted only where $IVT \geq 250\ kg\ m^{-1}\ s^{-1}$. ERA5 data were used to produce the plots. The Piedmont region is marked with the red box

As regards the convective precipitation in southern Piedmont on the 4th of November, the Meso-NH forecast reconstructs the dynamics of the event well, apart from the fact that the maximum value seems to be misplaced by a few tens of kilometres to the east of the actual position. What is important to stress is that convective cells are reconstructed in the lee side of coastal mountains in southern Piedmont, as can be appreciated by looking at the vertical cross sections in Fig. 6. Using a convection-permitting model, as suggested by Buzzi et al. (1998), was likely the key to achieving such a result. This is an improvement with respect to previous studies (Buzzi et al. (1998); Romero et al. (1998); Ferretti et al. (2000); Cassardo et al. (2002)), which lacked the reconstruction of precipitation patterns on both the north and south sides of the coastal mountains.

As regards the orographic precipitation in northern Piedmont on the 5th of November, the high-resolution and convection-permitting Meso-NH forecast does not add any new insights with respect to past numerical investigations. As found in previous studies, there is a fairly good consistency between model predictions and rain-gauges data (see Fig. 8). Large amounts of rainfall are predicted in the Alps in correspondence to mountain peaks, which seem to be unrealistic given the observations available (see data in Lionetti (1996) and Cassardo et al. (2002)). The overestimation of the model might be due to the implementation of the ICE3 microphysics scheme, which produces an excess of precipitating graupels or other hydrometeors. Rotunno and Ferretti (2001) suggested that the simpler Kessler scheme (Kessler 1969) contains the essential set of water categories relevant for the P94 case. This scheme takes into account three type of hydrometeors: vapour, cloud water and rain. However, a test Meso-NH simulation using the Kessler scheme provided results that do not differ very much from the ones presented here (map not shown). We give the results with the ICE3

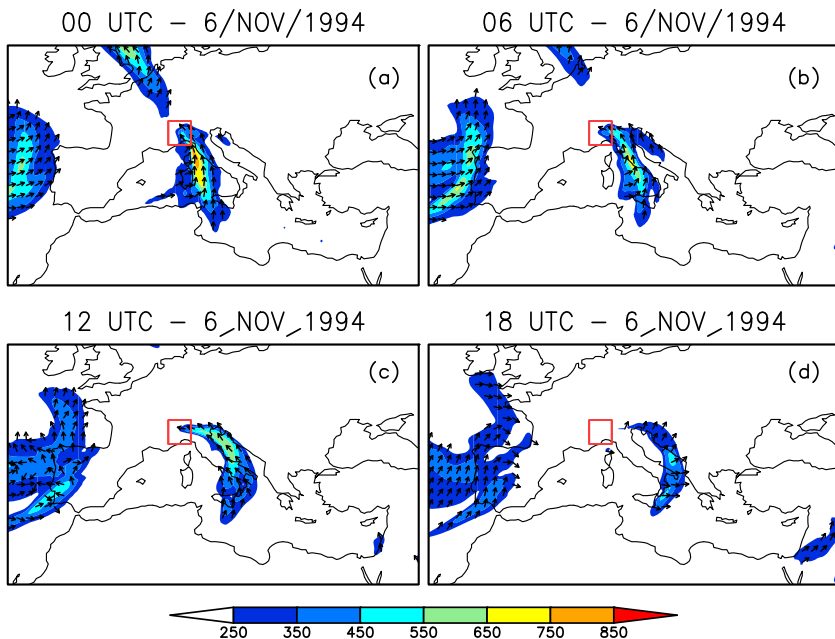


Fig. 10 Vertically integrated horizontal water vapour transport (IVT) values expressed in $kg\ m^{-1}\ s^{-1}$ for the four 6-h time steps on the 6th of November 1994: **a** 00 UTC, **b** 06 UTC, **c** 12 UTC and **d** 18 UTC. Wind vectors at 850-hPa isobaric level are plotted only where $IVT \geq 250\ kg\ m^{-1}\ s^{-1}$. ERA5 data were used to produce the plots. The Piedmont region is marked with the red box

scheme, because it is the most commonly used one-moment scheme in Meso-NH (Lac et al. 2018) and thus the results obtained can be compared with similar works or case studies. Moreover, it is more appropriate to describe the hydrometeors involved in the convective precipitation on the 4th of November as demonstrated by the vertical cross sections shown in Fig. 6.

We conclude the discussion on the Meso-NH simulations by speculating why longer forecasts than the ones presented here provide results that do not differ substantially from those shown in Figs. 4 and 7. We guess that one of the reasons lies in the improvements gained over the last 25 years by global NWP modelling. Indeed, in the paper by Petroliaigis et al. (1996), the authors found good results regarding the predictability of the P94 case. They found consistency (i.e. no sudden changes) among consecutive forecasts. The global analyses and forecasts we used to drive the Meso-NH simulations benefit from the improvements over the last years in terms of model cycle and data assimilation method. As regards the P94 case, such improvements further reduce any *jumpiness* in the data we used as compared with that present in the data of Petroliaigis et al. (1996). It follows that any subsequent medium-range (i.e. lead-times ≤ 72 h) regional model forecast is as reliable as a short-term (i.e. lead-times ≤ 24 h) one.

The IVT maps shown in Figs. 9 and 10 demonstrate that an AR landfall occurred during the P4 case and that it played an important role in controlling the storm-total precipitation in northern Piedmont. Following the scale proposed by Ralph et al. (2019), such an AR is in category 2 out of 5. In terms of hazardous impacts, a category 2 corresponds to “Mostly beneficial, but also hazardous” (Ralph et al. 2019). We stress the fact that this subjective

assessment was designed for the west coast of the USA for which the word “beneficial” stands for increased reservoir levels, drought relief, and water supply. For the P94 case, this terminology is inappropriate. For areas with complex topography, AR landfalls are often associated with large amounts of rainfall, which frequently lead to floods (Gimeno et al. 2014). What we can deduce from the presence of an AR during the P94 case is that it supplied the necessary contribution of moisture able to change the Froude number in the Alps (which is about 0.90 according to Doswell III et al. (1998)). This conclusion agrees well with the findings in Buzzi et al. (1998) and Cassardo et al. (2002), who demonstrated that the contribution of moisture was not due to the evaporation of air from the Mediterranean Sea. Furthermore, because ARs involve processes at the meso- α and β scales, this partially explains why the numerical investigations performed more than 25 years ago (listed in Table 1) were quite skilful in predicting the precipitation in the mountainous part of the region. One may argue that diverse algorithms for the detection of ARs take into account not only the IVT intensity and duration (as in Ralph et al. (2019)) but also criteria applied on integrated water vapour (IWV) and on the geographical extent of the area where IWV conditions are met. For instance, Ralph et al. (2004) and Neiman et al. (2008) used an objective identification algorithm that involves the imposition of three conditions: (i) IWV exceeds 20 mm, (ii) wind speeds in the lowest 2 km greater than 12.5 m s^{-1} and (iii) a long ($>2000 \text{ km}$) and narrow ($<1000 \text{ km}$) shape. For the P94 case, the conditions on the IWV and wind values are satisfied, whereas the condition on the extent of the area is not met (namely its length is less than 2000 km). Nevertheless, what we want to stress is that the water vapour transported meridionally across the mountainous area of Piedmont was sufficient to change the static stability of the air impinging the reliefs and thus favouring large amounts of rainfall. Indeed, Fig. 9 confirms the presence of a strong horizontal humidity gradient in the low-level airstreams affecting the Italian peninsula (Rotunno and Ferretti 2001). The western part of the flow is moist, whereas the eastern one is drier. This latter is deflected westward (i.e. to the left) over the Po Valley, following the mechanism of the barrier winds (Buzzi et al. (2014); Buzzi et al. (2020)). Such deflection causes a convergence with the flow over Piedmont, which is very humid. The moist flow is forced to rise over the drier one and upstream of the orographic barrier, reducing dynamically the height of the mountains to surmount. In other words, the lower the orographic barrier (i.e. the value of h in Eq. 1), the greater the Froude number.

The flooding of the Piedmont region in November 1994 is remembered because of its memorable impacts on the territory and the society. It drew the attention of the scientific community due to the atmospheric processes involved, which make this event a testbed to investigate orographic precipitation mechanisms. Past numerical experiments were able to capture most of the features of the event. However, we think that reforecasting past severe weather events by testing new models (e.g. convection-permitting), parametrisation (e.g. advanced microphysical schemes) and data (e.g. reanalyses) is valuable to better understand the forecasting capabilities of current systems.

Acknowledgements The Meso-NH model is freely available under the CeCILL license agreement. The author wishes to thank the model’s developers and the User Support for their help.

Data used to start and provide boundary conditions to the Meso-NH simulations were downloaded from the ECMWF MARS catalogue with experiment id “h6bg”.

The Copernicus Climate Change Service (C3S) is acknowledged for the ERA5 data, which were used to produce the maps in Figs. 1, 9 and 10.

Compliance with ethical standards

Conflict of interest The author declares that he has no conflict of interest.

References

- Buzzi A, Davolio S, Malguzzi P, Drofa O, Mastrangelo D (2014) Heavy rainfall episodes over Liguria in autumn 2011: numerical forecasting experiments. *Nat Hazards Earth Syst Sci* 14(5):1325
- Buzzi A, Di Muzio E, Malguzzi P (2020) Barrier winds in the Italian region and effects of moist processes. *Bulletin of Atmospheric Science and Technology*, 1–32
- Buzzi A, Foschini L (2000) Mesoscale meteorological features associated with heavy precipitation in the southern Alpine region. *Meteorol Atmos Phys* 72(2-4):131–146
- Buzzi A, Tartaglione N, Malguzzi P (1998) Numerical simulations of the 1994 Piedmont flood: role of orography and moist processes. *Mon Weather Rev* 126(9):2369–2383
- Caniaux G, Redelsperger JL, Lafore JP (1994) A numerical study of the stratiform region of a fast-moving squall line. Part I: general description and water and heat budgets. *J Atmos Sci* 51(14):2046–2074
- Cassardo C, Loglisci N, Gandini D, Qian MW, Niu G-Y, Ramieri P, Pelosini R, Longhetto A (2002) The flood of November 1994 in Piedmont, Italy: a quantitative analysis and simulation. *Hydrol Process* 16(6):1275–1299
- Doswell III CA, Ramis C, Romero R, Alonso S (1998) A diagnostic study of three heavy precipitation episodes in the western Mediterranean region. *Weather Forecast* 13(1):102–124
- Ebert EE (2009) Neighborhood verification: a strategy for rewarding close forecasts. *Weather Forecast* 24(6):1498–1510
- Ferretti R, Low-Nan S, Rotunno R (2000) Numerical simulations of the Piedmont flood of 4–6 November 1994. *Tellus A* 52(2):162–180
- Gimeno L, Nieto R, Vázquez M, Lavers DA (2014) Atmospheric rivers: a mini-review. *Front Earth Sci* 2:2
- Hagelin S, Son J, Swinbank R, McCabe A, Roberts N, Tennant W (2017) The Met Office convective-scale ensemble, MOGREPS-UK. *Q J Roy Meteorol Soc* 143(708):2846–2861
- Hersbach H, Bell W, Berrisford P, Horányi A, J MS, Nicolas J, Radu R, Schepers D, Simmons A, Soci C, Dee D (2019) Global reanalysis: goodbye ERA-Interim, hello ERA5. *ECMWF News1*, 17–24
- Hohenegger C, Walser A, Langhans W, Schär C (2008) Cloud-resolving ensemble simulations of the August 2005 Alpine flood. *Q J Roy Meteorol Soc* 134(633):889–904
- Jansa A, Genoves A, Garcia-Moya JA (2000) Western Mediterranean cyclones and heavy rain. Part 1: numerical experiment concerning the Piedmont flood case. *Meteorol.Appl* 7(4):323–333
- Kessler E (1969) On the distribution and continuity of water substance in atmospheric circulations. In: *On the distribution and continuity of water substance in atmospheric circulations*. Springer, pp 1–84
- Krichak SO, Feldstein SB, Alpert P, Gualdi S, Scoccimarro E, Yano JI (2016) Discussing the role of tropical and subtropical moisture sources in cold season extreme precipitation events in the Mediterranean region from a climate change perspective. *Nat Hazards Earth Syst Sci* 16(1):269
- Lac C, Chaboureaud JP, Masson V, Pinty JP, Tulet P, Escobar J, Leriche M, Barthe C, Aouizerats B, Augros C, et al. (2018) Overview of the meso-NH model version 5.4 and its applications. *Geosci Model Dev* 11(5):1929
- Lavers DA, Villarini G (2013) The nexus between atmospheric rivers and extreme precipitation across Europe. *Geophys Res Lett* 40(12):3259–3264
- Leutbecher M, Lock SJ, Ollinaho P, Lang ST, Balsamo G, Bechtold P, Bonavita M, Christensen HM, Diamantakis M, Dutra E, et al. (2017) Stochastic representations of model uncertainties at ECMWF: state of the art and future vision. *Q J Roy Meteorol Soc* 143(707):2315–2339
- Lionetti M (1996) The Italian floods of 4–6 November 1994. *Weather* 51(1):18–27
- Lunet T, Lac C, Auguste F, Visentin F, Masson V, Escobar J (2017) Combination of WENO and explicit Runge-Kutta methods for wind transport in the Meso-NH model. *Mon Weather Rev* 145(9):3817–3838
- Neiman PJ, Ralph FM, Wick GA, Lundquist JD, Dettinger MD (2008) Meteorological characteristics and overland precipitation impacts of atmospheric rivers affecting the West Coast of North America based on eight years of SSM/I satellite observations. *J Hydrometeorol* 9(1):22–47

- Nickerson EC, Richard E, Rosset R, Smith DR (1986) The numerical simulation of clouds, rains and airflow over the Vosges and Black Forest mountains: a meso- β model with parameterized microphysics. *Mon Weather Rev* 114(2):398–414
- Palmer TN (2001) A nonlinear dynamical perspective on model error: a proposal for non-local stochastic-dynamic parametrization in weather and climate prediction models. *Q J Roy Meteorol Soc* 127(572):279–304
- Peralta C, Ben Bouallègue Z, Theis SE, Gebhardt C, Buchhold M (2012) Accounting for initial condition uncertainties in COSMO-DE-EPS. *J Geophys Res Atmos* 117(D7):1–13
- Petroliaigis T, Buizza R, Lanzinger A, Palmer TN (1996) Extreme rainfall prediction using the European Centre for Medium-Range Weather Forecasts ensemble prediction system. *J Geophys Res Atmos* 101(D21):26227–26236
- Porcú F, Caracciolo C, Prodi F (2003) Cloud systems leading to flood events in Europe: an overview and classification. *Meteorol Appl* 10(3):217–227
- Ralph FM, Neiman PJ, Wick GA (2004) Satellite and CALJET aircraft observations of atmospheric rivers over the eastern North Pacific Ocean during the winter of 1997/98. *Mon Weather Rev* 132(7):1721–1745
- Ralph FM, Rutz JJ, Cordeira JM, Dettinger M, Anderson M, Reynolds D, Schick LJ, Smallcomb C (2019) A scale to characterize the strength and impacts of atmospheric rivers. *Bull Am Meteorol Soc* 100(2):269–289
- Raynaud L, Bouttier F (2016) Comparison of initial perturbation methods for ensemble prediction at convective scale. *Q J Roy Meteorol Soc* 142(695):854–866
- Roebber PJ (2009) Visualizing multiple measures of forecast quality. *Weather Forecast* 24(2):601–608
- Romero R, Ramis C, Alonso S, Doswell III CA, Stensrud DJ (1998) Mesoscale model simulations of three heavy precipitation events in the western Mediterranean region. *Mon Weather Rev* 126(7):1859–1881
- Rotunno R, Ferretti R (2001) Mechanisms of intense alpine rainfall. *J Atmos Sci* 58(13):1732–1749
- Rutz JJ, Steenburgh WJ, Ralph FM (2014) Climatological characteristics of atmospheric rivers and their inland penetration over the western United States. *Mon Weather Rev* 142(2):905–921
- Stohl A, Forster C, Sodemann H (2008) Remote sources of water vapor forming precipitation on the Norwegian west coast at 60 N - a tale of hurricanes and an atmospheric river. *J Geophys Res Atmos* 113(D5):1–13
- Sun J, Xue M, Wilson JW, Zawadzki I, Ballard SP, Onvlee-Hooimeyer J, Joe P, Barker DM, Li P-W, Golding B, et al. (2014) Use of NWP for nowcasting convective precipitation: recent progress and challenges. *Bull Am Meteorol Soc* 95(3):409–426
- Wilks DS (2011) *Statistical methods in the atmospheric sciences*, vol 100. Academic press, Cambridge
- Yano JJ, Ziemiański MZ, Cullen M, Termonia P, Onvlee J, Bengtsson L, Carrassi A, Davy R, Deluca A, Gray SL, et al. (2018) Scientific challenges of convective-scale numerical weather prediction. *Bull Am Meteorol Soc* 99(4):699–710
- Zhu Y, Newell RE (1998) A proposed algorithm for moisture fluxes from atmospheric rivers. *Mon Weather Rev* 126(3):725–735